NeuroImage 59 (2012) 1043–1051

Contents lists available at SciVerse ScienceDirect

NeuroImage

journal homepage: www.elsevier.com/locate/ynimg

Complex relationships between cerebral blood flow and brain atrophy in early Huntington's disease

J. Jean Chen *, David H. Salat, H. Diana Rosas

A.A. Martinos Center for Biomedical Imaging, Department of Neurology, Massachusetts General Hospital, Harvard Medical School, USA

ARTICLE INFO

Article history:
Received 10 March 2011
Revised 25 August 2011
Accepted 29 August 2011
Available online 16 September 2011

Keywords:
Huntington's disease (HD)
Pulsed arterial-spin labeling (PASL)
Magnetic resonance imaging (MRI)
Cerebral blood flow (CBF)
Cortical thickness

ABSTRACT

Alterations in cerebral blood flow (CBF) may play an important role in the pathophysiology of neurodegenerative disorders such as Huntington's disease (HD). While a few reports have suggested reductions in CBF in HD, little is known about their extent and whether, or how, they might be related to atrophy and to clinical symptoms. We used pulsed arterial-spin labeling MRI in conjunction with high-resolution anatomical MRI to non-invasively measure regional CBF in 17 early stage HD subjects and 41 age- and gender-matched healthy controls. We found profound yet heterogeneous CBF reductions in the cortex, extending to the sensorimotor, paracentral, inferior temporal and lateral occipital regions, with sparing of the neighboring postcentral gyrus, insula and medial occipital areas. As expected, CBF in subcortical regions was also profoundly reduced, and to a similar degree. Unexpectedly, however, the association between CBF reductions and regional atrophy was complex, the two being directly associated in certain areas but not with others. In contrast, CBF was associated with performance on the Stroop, suggesting a potentially important role for alterations in CBF in cognitive deficits in HD. The work described here may have broad-reaching implications for our understanding of HD pathogenesis, progression and emerging therapies.

Introduction

Alterations in cerebral blood flow (CBF) have been described in brain aging (Chen et al., 2011) and in several neurodegenerative disorders, including Alzheimer's disease (AD) (Iadecola, 2003; Tosun et al., 2010), Parkinson's disease (PD) (Borghammer et al., 2010; Théberge, 2008) and Huntington's disease (HD) (Harris et al., 1999; Ma and Eidelberg, 2007), suggesting important and likely early commonalities in otherwise distinct pathophysiological processes. For instance, in AD, perturbations in microvascular flow, believed to be related to the over-expression of amyloid precursor protein, have been shown to precede the development of neuronal dysfunction, leading to speculations that alterations in CBF may play important roles in both progression and clinical expression.

HD is a progressive neurodegenerative disorder which causes severe cognitive dysfunction, psychiatric disturbances and a movement disorder characterized by the presence of involuntary movements as well as altered motor control. In HD, the accumulation of a mutant form of "huntingtin", a protein of unknown function found heterogeneously in neurons throughout the brain, sets in motion a cascade of pathological events that eventually lead from neuronal dysfunction to neuronal death. Perturbations in cerebral glucose consumption (CMRglu) have been shown both with positron emission tomography (PET) (Ciarmiello et al., 2006b; Feigin et al., 2001; Kuwert et al., 1993) and single-photon emissions computed tomography (SPECT) (Sax et al., 1996) in early HD, beginning during the motor premanifest period, suggesting a potential role of altered cerebral blood flow in the pathophysiology of HD. In addition, several studies, primarily using SPECT (Aylward et al., 1997; Ciarmiello et al., 2006b; Deckel et al., 2000; Harris et al., 1999; Hasselbalch et al., 1992; Hobbs et al., 2009; Jernigan et al., 1991; Jurgens et al., 2008; Kassubek et al., 2005; Selemon et al., 2004; Sotrel et al., 1991; Wild et al., 2009), or X-ray computed tomography (CT) have also suggested alterations in both cortical and subcortical CBF. However, both SPECT and CT provide relatively low spatial resolution and/or tissue contrast. We hypothesized that alterations in CBF might in fact be more extensive but reflect the regional selectivity that has been previously reported in HD, affecting both the basal ganglia and select cortical regions (Aylward et al., 1997; Ciarmiello et al., 2006b; Deckel et al., 2000; Harris et al., 1999; Hasselbalch et al., 1992; Hobbs et al., 2009; Jernigan et al., 1991; Jurgens et al., 2008; Kassubek et al., 2005; Selemon et al., 2004; Sotrel et al., 1991; Rosas et al., 2008; Wild et al., 2009). It is noteworthy that those cortical regions suggested to degenerate early in HD are precisely those known to have high energetic demands, including primary cortical regions (Hobbs et al., 2009; Jech et al., 2007; Rosas et al., 2003, 2008; Stoffers et al., 2010); as such, even minor perturbations in CBF would potentially result in increased susceptibility to oxidative stress. Indeed, reductions in CBF have been shown to enhance oxidative stress, which then may further promote formation of radicals and neurodegeneration (Browne and Beal, 2006;

* Corresponding author at: A. A. Martinos Center for Biomedical Imaging, Massachusetts General Hospital, Harvard Medical School, Charlestown, MA, 02129, USA. Fax: +1 617 724 1227.
E-mail address: jjchen@nmr.mgh.harvard.edu (J.J. Chen).

1053-8119/$ – see front matter © 2011 Elsevier Inc. All rights reserved.
doi:10.1016/j.neuroimage.2011.08.112

Browne et al., 1999; Deckel et al., 1998, 2000; Gonzalez-Zulueta et al., 1998; Reijonen et al., 2010; Squitieri et al., 2003; Underwood et al., 2010).

In this work, we used a novel, non-invasive pulsed arterial-spin labeling (PASL) magnetic resonance imaging (MRI) technique to evaluate regional blood flow in HD and healthy controls, and to examine their relationship with regional atrophy. PASL provides superior spatial resolution and sensitivity relative to traditional techniques, and permits the acquisition of perfusion data in the same session as high-resolution anatomical MRI. Our data demonstrate that alterations in cerebral perfusion are indeed topologically distinct and appear to be substantively independent of tissue atrophy. The presence of early perfusion deficits in regions with no associated measurable atrophy suggests an important role of perfusion abnormalities in the pathophysiology and regional selectivity of HD, and may be an important consideration for the development of novel HD therapeutics.

Materials and methods

Participants

Seventeen individuals with clinically diagnosed early Huntington's disease (HD, age = 50.3 ± 5.5 years) and forty-one age-matched healthy controls (CTL, age = 50.0 ± 5.8) were imaged (see Table 1 for demographic information). HD participants were recruited through the Massachusetts General Hospital (MGH) Movement Disorders Clinic; controls were recruited from the MGH and local community. HD participants were assessed by a neurologist with expertise in HD (HDR). A diagnosis of HD was based on the presence of an unequivocal movement disorder as well as a positive family history and known CAG repeat expansion. Disease severity was assessed through the total functional capacity (TFC), measured from the Unified Huntington's Disease Rating Scale (UHDRS) (Huntington Study Group, 1996). Controls were healthy, and had no history of neurological or psychiatric symptoms. All study protocols were approved by the Massachusetts General Hospital Internal Review Board (IRB), and the experiments were performed with the understanding and written consent of each participant, according to IRB guidelines.

MRI acquisition

All images were acquired using a Siemens Magnetom Trio 3 Tesla system (Siemens, Erlangen, Germany). The scans employed 12-channel phased-array head coil reception and body-coil transmission. The total scan time was ~50 min. A 3D T1-weighted scan was acquired using multi-echo MPRAGE (van der Kouwe et al., 2008), with 1 mm in-plane resolution, TR = 2530 ms, TI = 1000 ms, TE = 1.64, 3.50 5.36 and 7.22 ms, FOV = 256×256 mm (sagittal), matrix size = 256×192, 175 slices, slice thickness = 1.33 mm, bandwidth = 651 Hz/pixel, GRAPPA acceleration factor of 2.

Two pulsed arterial-spin labeling (PASL) datasets were obtained for each subject using the FAIR QUIPSS II technique (Wang et al., 2002). This permitted the assessment of across-run repeatability in all subjects. A slice-selective frequency-offset corrected inversion (FOCI) pulse was applied during tag and control, the latter scan acquired in the absence of slab-selective gradients. The tag and control labeling thicknesses were 140 mm and 340 mm, respectively, leaving 100 mm margins at either end of the imaging slab to ensure optimal inversion profile. The QUIPSS II saturation pulse was applied to a 100 mm slab inferior to the imaging region with a 10 mm gap between the adjacent edges of the saturation and imaging slabs. Flow crusher gradients were applied with a threshold of 100 cm/s. Other imaging parameters were: 64×64 matrix, 24 slices, with a voxel size = 3.4×3.4×5 mm^3. Two PASL acquisitions of 104 frames were acquired for each subject using a TI1 of 600 ms and TI2 of 1600 ms, chosen to accommodate a wide range of flow rates. The scans used a repetition time (TR) of 4 s, and an echo-time of 12 ms, made possible by the current implementation of ¾ partial Fourier echo-planar imaging (EPI) readout, which enabled the minimization of BOLD effects and the reduction of susceptibility-related geometric distortions. The acquisition time per slice was 42 ms. A 2D gradient-echo EPI sequence of the same TE and spatial resolution was used in a calibration scan (with TR set to 10 s) to estimate the equilibrium magnetization of arterial blood.

Data processing

Quantitative CBF computation

The raw PASL time-series were motion- and drift-corrected using FLIRT registration software (publicly available at http://fsl.fmrib.ox.ac.uk/fsl/flirt), and subsequently divided into 52 tag-control pairs for each acquisition. To minimize BOLD-contamination, the tag-control difference images were calculated using surround subtraction (Lu et al., 2006). Longitudinal (T1) relaxation due to the slice-dependent transit delay was also compensated based on the per-slice acquisition time. The PASL volumes were then averaged across all frames and datasets to maximize signal-to-noise, and subsequently quantitative CBF maps were obtained according to the single-compartment Standard Kinetic Model (Buxton et al., 1998; Wang et al., 2002). The equilibrium arterial-blood magnetization was computed as the intensity in the calibration scan adjusted for longitudinal (T_1) and transverse relaxation (T_2^*) differences as well as blood–tissue water partition coefficient (λ). Typical values for proton density, λ, T_1 and T_2^* were assumed for all gray matter based on prior literature, as described in (Cavuşoğlu et al., 2009). The labeling efficiency was assumed to be 98% (Wong et al., 1998a); the mean CBF estimation reliability was greater than 93%, with no significant variation across cortical and subcortical structures.

Structural analysis and cortical thickness computation

All structural image pre-processing steps were performed on the root-mean-square reconstruction of the multi-echo MPRAGE images using the FreeSurfer image processing and analysis package (publicly available at http://surfer.nmr.mgh.harvard.edu), as has been described previously (Chen et al., 2011; Rosas et al., 2008; Salat et al., submitted for publication). The procedure includes removal of non-brain tissue using a hybrid watershed/surface deformation procedure (Segonne et al., 2004), automated transformation into the MNI152 standard space, intensity normalization (Sled et al., 1998), tessellation of the gray matter white matter boundary, automated topology correction (Segonne et al., 2007), and surface deformation following intensity gradients to optimally place the gray/white and gray/CSF borders at the location

Table 1
Participant demographics and clinical-psychological scores (mean ± standard deviation). (HD = Huntington's patients; CTL = healthy controls; M = men; W = women; CAG = cytosine–adenine–guanine; Stroop = UHDRS Stroop colour-word score; TFC = total functional capacity).

Group	N	Age [year]	CAG	Symbol digit	Stroop	Verbal fluency	TFC
HD	17 (7 M/10 W)	50.3 ± 5.5	43.8 ± 1.7	28.4 ± 14.1	29.8 ± 12.8	26.1 ± 13.6	9.1 ± 2.7
CTL	41 (17 M/24 W)	50.0 ± 5.8	N/A	45.2 ± 11.1	44.9 ± 11.1	45.2 ± 10.5	N/A

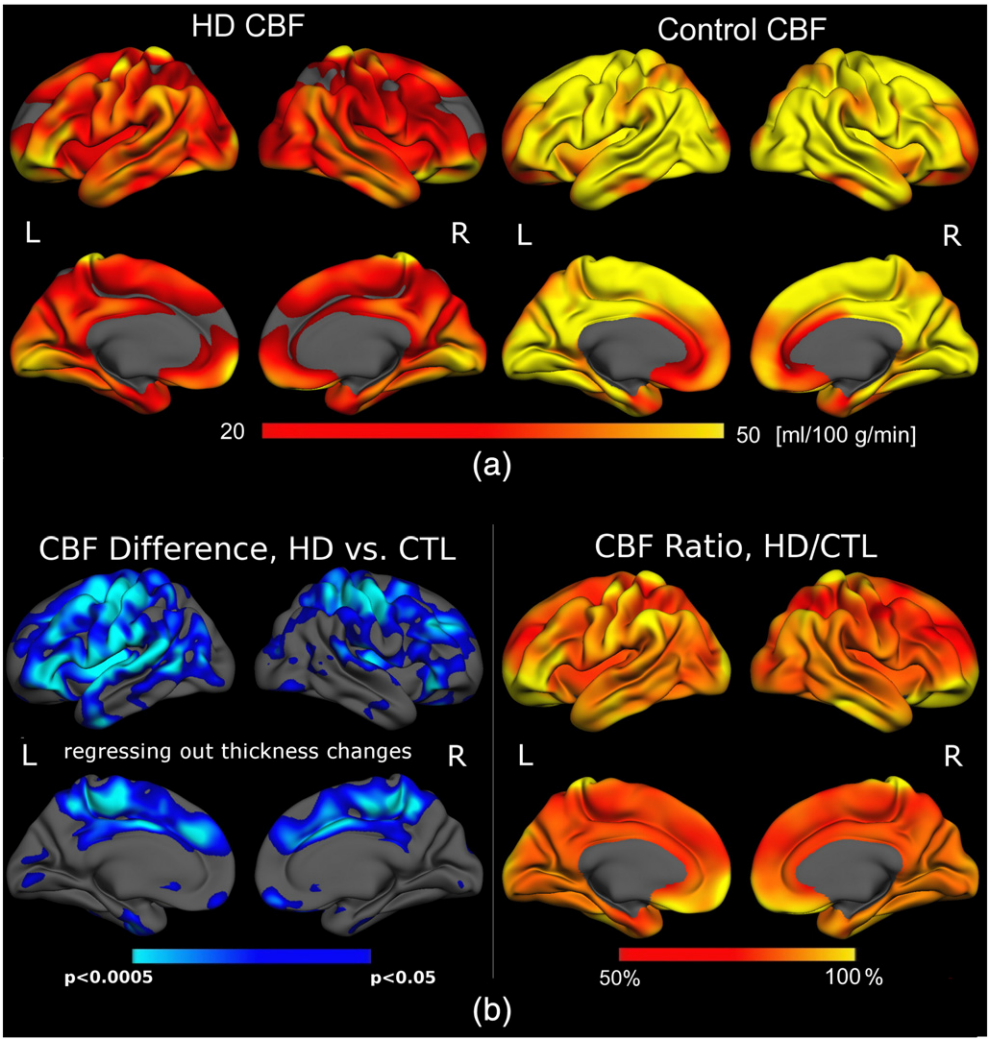

Fig. 1. Cortical mapping of quantitative CBF for early HD patients and controls. (a) CBF in HD subjects (left) was on the average of 48.4 ± 12.5 ml/100 g/min over the entire cortex, markedly lower than CBF in controls (right), averaging 62.9 ± 9.7 ml/100 g/min. (b) Left: CBF was significantly reduced in the HD group (shown in blue) relative to the control population (adjusted for multiple comparisons). CBF was primarily compromised in the superior frontal, insular, lateral occipital and posterior cingulate regions, with the inferior temporal and medial occipital cortical regions comparatively "spared". Right: Ratio between the mean CBF in the HD and control groups, showing regional CBF to be reduced by as much as 50% in the HD group.

where the greatest shift in intensity defines the transition to the other tissue class (Fischl and Dale, 2000).

Estimates of cortical thickness, calculated as the closest distance from the gray/white boundary to the gray/CSF (cerebrospinal fluid) boundary at each vertex on the tessellated surface (Fischl and Dale, 2000), as described previously. In addition, cortical and subcortical regions of interest were delineated as described previously (Fischl et al., 2004b).

Group analyses

The PASL data were resampled to 1 mm^3 spatial resolution and registered to the native-space anatomical images using boundary-based registration (Greve and Fischl, 2009). The mid-frame of the motion- and drift-corrected PASL time-series was chosen as the template image. ASL-to-anatomical registration was performed by minimizing the misalignment between the cortical gray-white boundaries in the anatomical and PASL template images through 6–12 degree affine transforms. This method is minimally sensitive to differences in contrast and intensity non-uniformity in the two datasets, and the procedure benefited from the minimization of geometric distortions in the PASL images owing to the use of the short-TE partial-Fourier acquisition. This method has been shown to provide reproducible CBF estimates across runs (Chen et al., 2011).

To facilitate group-analysis, the anatomical-registered PASL data were sampled onto the spherical surface, at a depth of 50% into the cortical ribbon. This approach minimized the inclusion of voxels contaminated with white-matter or CSF. Group-mean CBF maps were generated using non-rigid high-dimensional spherical averaging (Fischl et al., 1999). General linear model-based statistical tests were performed based on smoothing along the surface using a circularly symmetric Gaussian kernel with a full-width at half-maximum (FWHM) of 10 mm, and the results were corrected for multiple comparisons using Random Field Theory (Hagler et al., 2006; Worsley et al., 2004).

To evaluate the relationship between regional reductions in CBF and cortical atrophy, spatial overlap maps were generated. Significant effects of HD were computed using *t*-tests, and that of the inter-group comparisons were all performed using multi-factorial analysis of variance (ANOVA), with gender as a covariate.

The cortical regions exhibiting the most significant HD-induced CBF decrease were demarcated for individual ROI analysis; CBF and cortical thickness changes were compared within this set of regions. Subcortical gray-matter structures were individually segmented in native space, as described previously (Fischl et al., 2004a,b), and their respective mean CBF values extracted in both hemispheres. All structural volume measures were corrected for estimated total intracranial volume using the atlas-scaling and covariance approach (Buckner et al., 2004). All

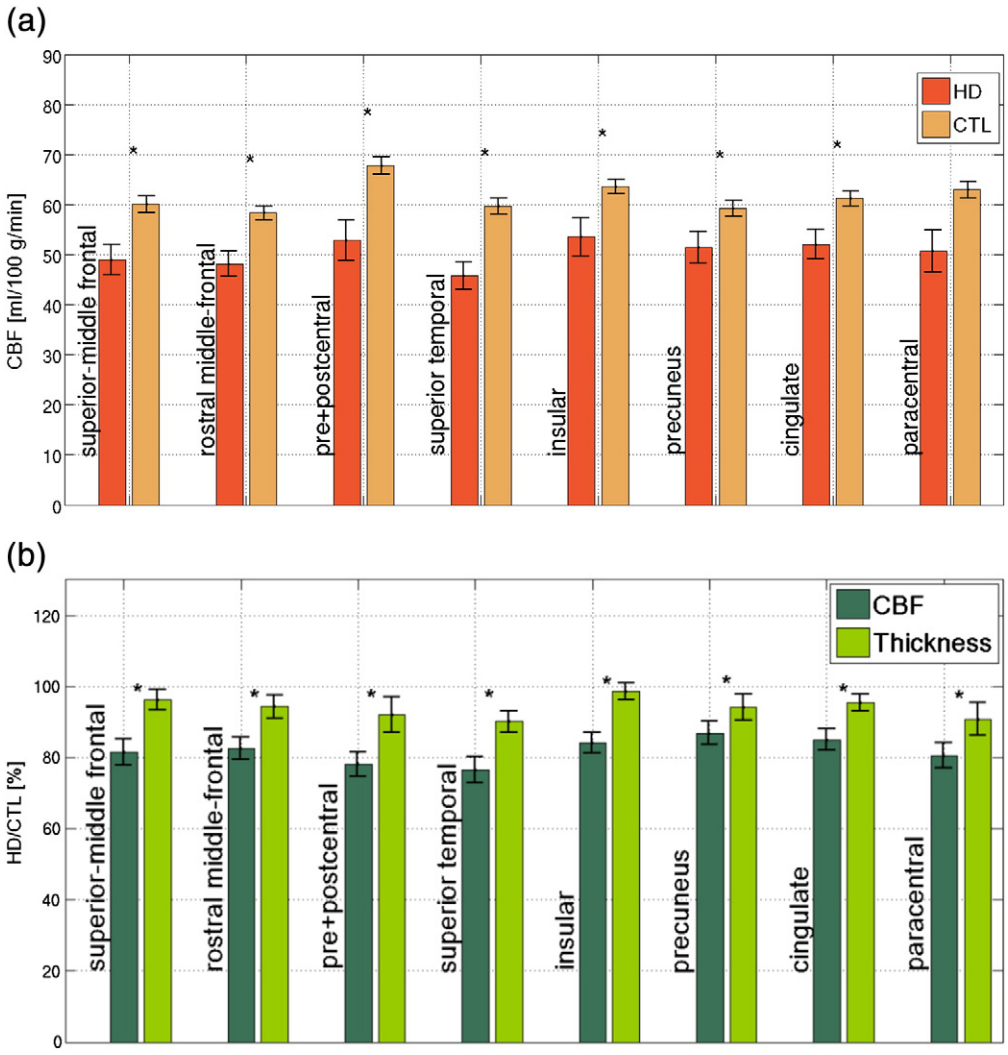

Fig. 2. Region-of-Interest (ROI) analysis in regions found to be the most affected in HD. While the normative resting CBF varies across the cortex, a similar degree of proportionate CBF reduction in HD was observed across all ROIs. The error bars represent standard error, and significant differences are denoted by asterisks ($p<0.05$). In many ROIs, reductions in cortical CBF in HD subjects exceed the degree of concurrent cortical thinning in the same regions, suggesting that the two were not entirely associated. The error bars represent standard error, and significant differences are denoted by asterisks ($p<0.05$).

segmented ROI masks were eroded by 1 mm around the perimeter to minimize partial-volume contamination. Mean CBF values across ROIs were computed in native space, and compared between HD and control (CTL) participants, using structural volume as a covariate.

Results

Quantitative cortical CBF measurements for HD subjects and the age- and sex-matched control group (CTL) were generated in multi-slice mode (see Supplementary materials), and mapped onto cortical surface models (Fig. 1a). In order to account for the potential contribution of partial volume effects on PASL measurements, the cortical thickness at each vertex was regressed out. Even following this step, significant reductions in CBF were still present in superior frontal, insular, paracentral, lateral-temporal and lateral-occipital areas, suggesting at least some independence between the two measures (Fig. 1b, left). HD subjects demonstrated CBF reductions of as much as 50% relative to controls (Fig. 1b, right).

Table 2
Group-mean CBF and cortical thickness measurements (mean ± standard deviation) in the cortical ROIs found to be most affected in HD subjects.

Region	CBF				Cortical thickness
	HD [ml/100 g/min]	CTL [ml/100 g/min]	HD<CTL	HD/CTL [%]	HD/CTL [%]
Superior-middle temporal	49.0 ± 3.0	60.1 ± 1.7	$p=0.001$	81.5 ± 3.6	96.2 ± 2.9
Rostral middle-frontal	48.2 ± 2.5	58.3 ± 1.4	$p<0.001$	82.6 ± 3.0	94.4 ± 3.2
Pre- and postcentral	52.9 ± 4.0	67.8 ± 1.7	$p=0.0001$	78.0 ± 3.4	92.0 ± 5.1
Paracentral	50.7 ± 4.2	62.9 ± 1.7	$p=0.001$	80.6 ± 3.5	98.7 ± 4.5
Superior temporal	45.8 ± 2.8	59.7 ± 1.6	$p<0.0001$	76.7 ± 3.7	94.2 ± 3.1
Insula	53.5 ± 3.8	63.6 ± 1.4	$p<0.01$	84.2 ± 2.8	95.4 ± 2.3
Precuneus	51.5 ± 3.2	59.2 ± 1.6	$p<0.05$	86.9 ± 3.3	90.8 ± 3.6
Cingulate	52.1 ± 2.9	61.2 ± 1.5	$p<0.05$	85.1 ± 2.9	90.1 ± 2.4

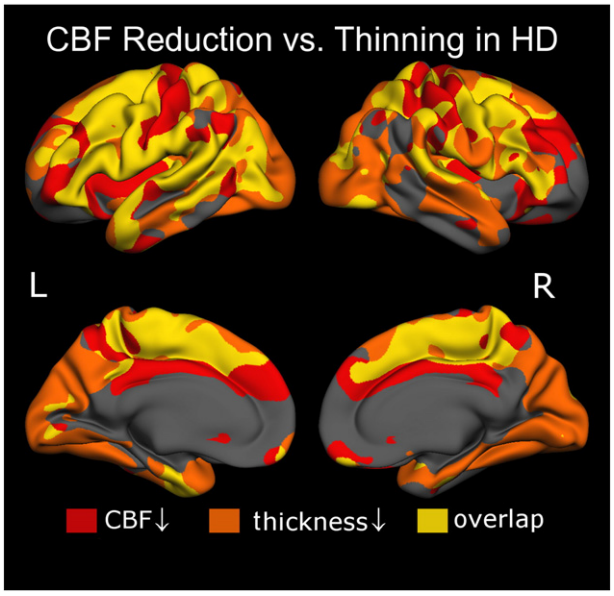

Fig. 3. Regional associations and dissociations between CBF and cortical thickness reductions in HD. CBF reductions were present across the cortical mantle, most prominently in the medial superior-frontal cortex, superior temporal gyrus and selectively in the occipital lobe. CBF reduction (red) and cortical thinning (orange) were associated (overlap shown in yellow) in the superior frontal, precentral, lateral occipital and posterior cingulate regions. On the other hand, spatial mismatches between the CBF and cortical thickness effects were evident in the insula, medial frontal and postcentral gyri as well as the lateral occipital lobe.

CBF differences between patients and controls in the most affected cortical regions are summarized in Fig. 2a. While the normative resting CBF appeared to vary across the cortex in both HD and controls, CBF in HD subjects appeared to be proportionately reduced across all ROIs. This was further supported by the HD/CTL CBF ratios, which did not vary significantly across the ROIs (Fig. 2b), but which consistently demonstrated that reductions in CBF exceeded the magnitude of concurrent cortical thinning (as the ratio of HDs to CTLs was lower for CBF than for thickness). CBF values for respective ROIs and the corresponding significance values are summarized in Table 2.

The overall distribution of relative "association" and "dissociation" between CBF and cortical thinning are better illustrated by the conjunction/disjunction analysis in Fig. 3. CBF reduction and cortical thinning were directly associated in superior frontal, precentral, lateral occipital and posterior cingulate regions. However, the two appeared to be dissociated in the postcentral gyrus and the insula. Likewise, in the lateral occipital lobe as well as portions of the temporal and cingulate cortices, thinning was significant without a corresponding reduction in CBF.

CBF in the HD group was also significantly reduced in the caudate, putamen, but paradoxically elevated in the pallidum relative to the controls (Fig. 4a, $p<0.001$ in all cases). The results are detailed in Table 3. There were no differences in CBF between HDs and controls in the thalamus, amygdala or hippocampus. As expected, significant volume reductions were present in HD subjects in the caudate, putamen, pallidum, thalamus, amygdala and hippocampus; in these regions, percent volume loss generally exceeded percent CBF reduction in HD (Fig. 4b).

We also evaluated the relationship between CBF and scores on the UHDRS cognitive battery. We found a significant direct correlation between CBF (not thickness) and performance on the UHDRS Stroop Colour Word, suggesting that early changes in CBF may play an important role in cognitive dysfunction in early HD (Fig. 5). In contrast, no significant association was observed between CBF and the CAG repeat length (Ravina et al., 2008).

Discussion

Using PASL, a novel, non-invasive quantitative perfusion imaging technique new to clinical applications (Detre et al., 2009) we found significant hypoperfusion in the HD group over much of the cortex. In some regions, including the frontotemporal, sensori-motor, occipital and cingulate areas, the maximum reduction in CBF reached 50% of control CBF values, while less significant reductions were associated with the insular and precuneal regions. Both the magnitude and the distribution of reductions in CBF in our HD subjects exceed those reported previously using SPECT and CT (Hasselbalch et al., 1992; Tanahashi et al., 1985; Weinberger et al., 1988). CBF estimates in controls are consistent with values in the PET and MRI literature (Calamante et al., 1999; Çavuşoğlu et al., 2009; Leenders et al., 1990; Shin et al., 2007), and particularly with prior findings using PASL (Wong et al., 1998a,b; Ye et al., 1997; Zou et al., 2009) and CASL (Lee et al., 2009; Zou et al., 2009) supporting the validity of our findings.

A more complicated pattern of perfusion abnormalities was present in the striatum. While CBF was reduced in both the caudate and putamen, as has been reported previously (Deckel et al., 2000; Ginovart et al., 1997; Harris et al., 1999; Hasselbalch et al., 1992; Ma and Eidelberg, 2007; Tanahashi et al., 1985), we found a paradoxical CBF increase in the pallidum. Early changes in the pallidum have been reported, including during the motor premanifest period (Politis et al., 2011; van den Bogaard et al., 2011). Loss of substance P and cannabinoid-1 receptors in the globus pallidus (Allen et al., 2009) modulate increases in GABA (gamma-aminobutyric acid) receptors (both $GABA_A$ and $GABA_B$) in response to the loss of GABAergic neurons in the globus pallidus in HD, and GABA levels have been found to inversely correlate with BOLD reactivity (Donahue et al., 2010). Hence, increases in CBF in the pallidum may reflect early loss of GABAergic neurons. However, our observation may also reflect an interesting compensatory response in the pallidum in face of striatal hypoperfusion. It is noteworthy that the cortical ROIs and in basal ganglia demonstrated similar levels of CBF reduction.

Of further note, cortical areas with high metabolic activity relative to the global average (c.f. Buckner et al., 2005; Leenders et al., 1990) appear to be the most severely and earliest affected in HD, parenthetically demonstrating the most significant reductions in CBF. Perturbations in microvascular flow regulation, which have been shown to precede the development of neuronal dysfunction in mouse models of AD (Iadecola, 2003), has contributed to speculations that the cerebral endothelium (potentially disrupted by amyloid deposition in AD) may serve as an endocrine organ that actively exchanges signaling mediators and trophic factors with gray and white matter (Arai and Lo, 2009; Dugas et al., 2008; Guo et al., 2008; Varga et al., 2009). While there have been no specific reports of effects of mutant huntingtin on the endothelium, the mutant huntingtin protein has been shown to directly affect expression and activity of endothelial nitric oxide synthase, and as such, reductions in vascular velocity and reactivity would not be entirely surprising (Deckel et al., 1998).

Altered metabolism and its consequent excitotoxicity, together with regional hypoperfusion, may tip the balance in vulnerable neuronal populations, and contribute to neuronal death. Alterations in metabolism and energetic dysfunction are, indeed, known to occur in HD — these include primary alterations of the electron transport chain as well as impaired energy metabolism leading to mitochondrial dysfunction (Browne and Beal, 2006; Feany and La Spada, 2003; Kim et al., 2010b; Powers et al., 2007). Reductions in glucose metabolism may reflect altered neural activity, either as a primary cause or secondary effect of hypoperfusion. In fact, metabolic disturbances, including reductions in striatal glycolysis (Powers et al., 2007) and creatine kinase have been reported in pre-manifest HD subjects (Kim et al., 2010a). In addition, the bilateral hypoperfusion in the striatum, cingulate and temporal regions coincide with decreased glucose metabolism measured in the

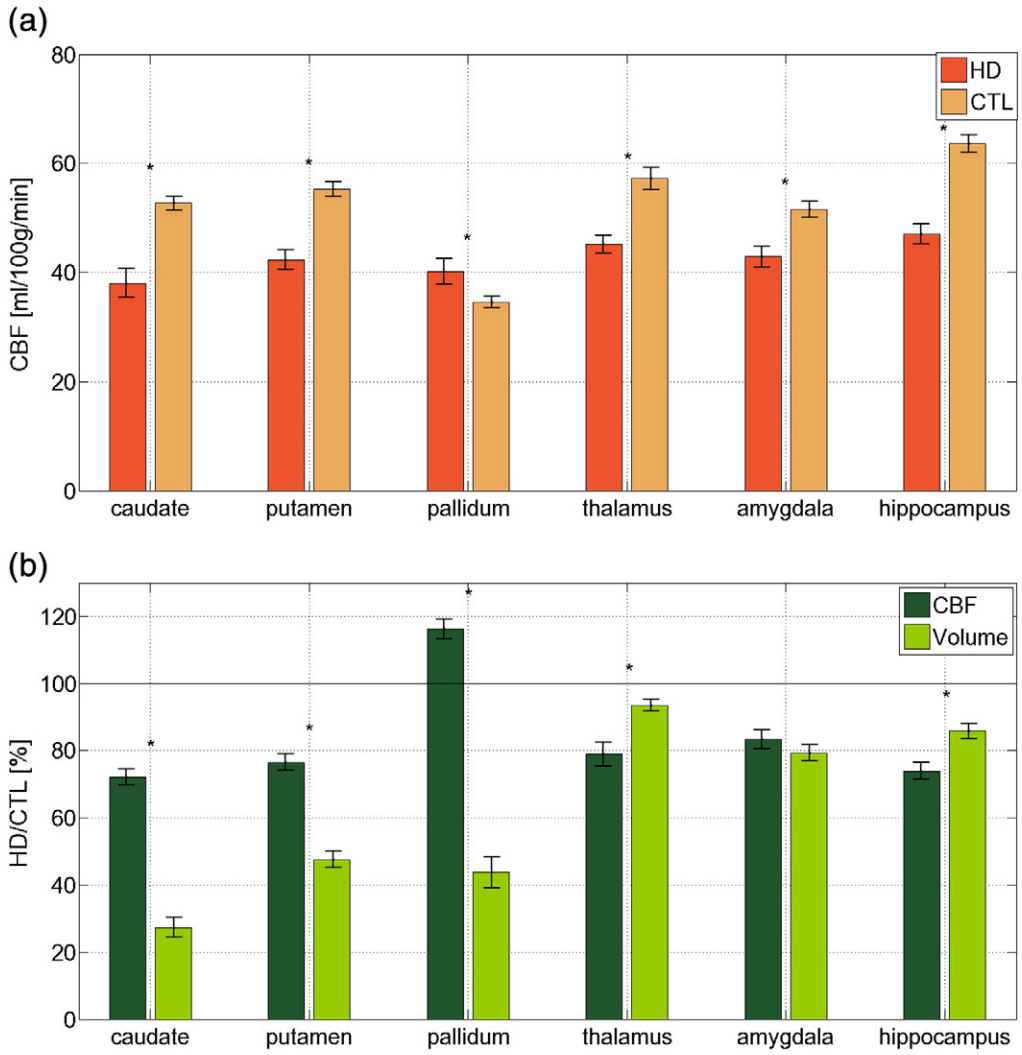

Fig. 4. CBF alterations in the basal ganglia, thalamus, amygdala and hippocampus. HD-related CBF reduction was present in the caudate and putamen. Paradoxically, pallidal CBF was elevated in the HD group. The degree of CBF reduction in the basal ganglia was comparable to that found in the cortical ROIs. The error bars represent standard error, and significant differences are denoted by asterisks ($p<0.05$). In the majority of subcortical gray-matter structures, the fractional loss of tissue volume exceeded the percent CBF reduction in the HD population. The error bars represent standard error, and significant differences are denoted by asterisks ($p<0.05$).

same regions using PET (Antonini et al., 1996; Ciarmiello et al., 2006a; Ma and Eidelberg, 2007; Powers et al., 2007), and could in part account for decreases in dopamine transporter binding (Ginovart et al., 1997).

We noticed that the distribution of reduction in CBF was not always accompanied by significant regional atrophy. This was particularly evident in the motor cortex, insula, precuneus, cingulate and lateral occipital cortices. In other cortical regions, including the medial superior-frontal cortex, superior temporal gyrus and medial occipital lobe, regions previously reported as significantly thinned in HD (Rosas et al., 2008), both CBF reduction and atrophy were observed; however, reductions in CBF far exceeded the degree of cortical atrophy. These observations may suggest that there is a dissociation between neurodegeneration and hypoperfusion, and that in other areas, hypoperfusion may reflect early neuronal dysfunction prior to measurable atrophy (Nopoulos et al., 2010; Rosas et al., 2008). However, the degree of tissue volume loss exceeded reductions CBF in temporal and occipital cortices as well as in the striatum suggesting potentially independent structural and vascular pathologic mechanisms at work. Clearly, longitudinal evaluation of how perfusion changes over the course of disease, beginning during the pre-manifest period, could facilitate our understanding of the relative contributions of reductions in CBF to neurodegeneration and to early clinical symptoms in HD.

Table 3
Group-mean CBF and structural volume measurements (mean ± standard deviation) in select cortical and subcortical structures.

Structure	CBF				Structural volume
	HD [ml/100 g/min]	CTL [ml/100 g/min]	HD<CTL	HD/CTL [%]	HD/CTL [%]
Caudate	38.0 ± 2.6	52.7 ± 1.2	$p<0.01$	72.9 ± 4.7	27.3 ± 3.2
Putamen	42.3 ± 1.8	55.3 ± 1.3	$p<0.0001$	51.8 ± 4.7	47.6 ± 2.7
Pallidum	40.2 ± 2.3	34.6 ± 1.0	$p=0.01$	95.4 ± 4.0	43.8 ± 4.6
Thalamus	45.2 ± 1.6	57.2 ± 2.1	$p<0.0001$	78.3 ± 5.7	93.5 ± 1.7
Amygdala	42.9 ± 1.9	51.5 ± 1.5	$p<0.0001$	82.4 ± 5.0	79.3 ± 2.5
Hippocampus	47.1 ± 1.8	63.6 ± 1.6	$p<0.0001$	73.7 ± 5.0	86.9 ± 2.3

Reductions of CBF in the insula and precuneus have not been demonstrated previously in HD. It is of note that these regions have been associated with memory and emotional processing, domains that are significantly affected in HD (Ruocco et al., 2010; Walker, 2007), supporting a potentially important role of reduced cerebral perfusion in early emotional and cognitive deficits, which has thus far been poorly explained by measurable atrophy. We indeed found a significant association between performance on Stroop Colour Word (Lemiere et al., 2004; Rosas et al., 2005), and reductions in CBF, but not cortical thickness, in

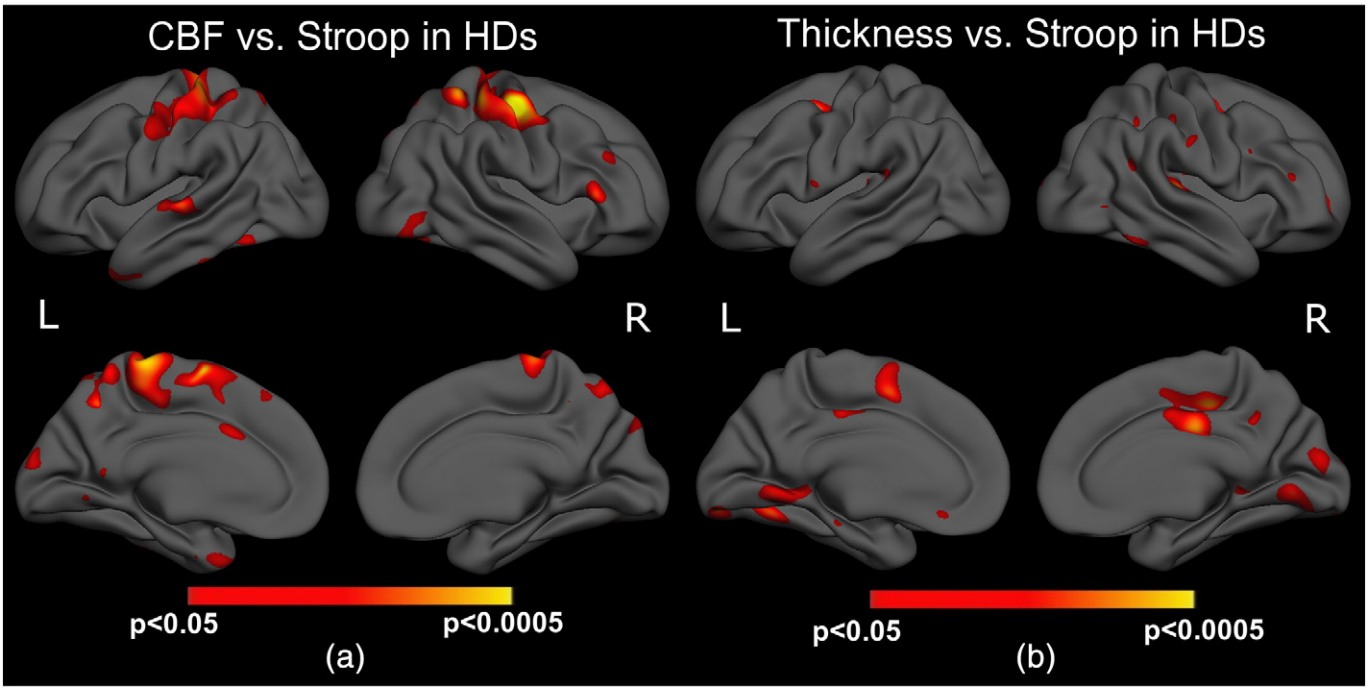

Fig. 5. Relationship between CBF, cortical thickness and Stroop Colour Word performance. Better Stroop performance was directly correlated with CBF regionally (a), while cortical thickness exhibited a less significant association to Stroop score (b).

regions that have been shown to be functionally associated with this task (Adleman et al., 2002), suggesting an important role of altered CBF in some of the cognitive deficits in HD. However, much remains to be done to fully elucidate the association between alterations in CBF and neuronal dysfunction in HD. MRI strategies combining morphometric and diffusion-based data are also promising ways to probe brain dysfunction in HD, and will be employed in our future studies to elucidate the disease mechanism.

The work presented here is novel for several reasons. The methods used in this study reflect a significant advance over the conventionally used approaches. Using a surface-based algorithm in native space permitted the minimization of partial-volume related confounds, which have been widely associated with PASL perfusion measurements, and also permitted appropriate and accurate intravoxel evaluation of the effect of atrophy on CBF measures. More importantly, this is the first study to examine the relationship between perfusion and tissue integrity in HD; a similar "uncoupling" has been demonstrated in AD, suggesting a potential common mechanism in neurodegenerative diseases (Tosun et al., 2010). Nonetheless, the current method does not involve an explicit correction for partial-volume effects in ASL, which is an area of active research in both ASL and PET literature (Asllani et al., 2008; Aston et al., 2002; Tosun et al., 2010). Finally, future studies will involve larger cohorts, as well as target longitudinal validation of the current findings in pre-symptomatic gene carriers.

Our perfusion measurements were obtained using PASL, which has been known to be sensitive to arterial transit delay, which may be lengthened in HD pathology. In addition, in the healthy brain, inferior regions are reportedly associated with longer transit delays than the superior half (Qiu et al., 2010), while relatively long delays have consistently been observed in select brain areas, including the frontal and occipital lobes (MacIntosh et al., 2010). As these factors are important determinants of CBF accuracy, our PASL parameters were chosen to minimize velocity-related bias. Specifically, a relatively short TI_1 of 600 ms facilitated the minimization of bolus-width sensitivity even for rapid flow, common to younger subjects, while a TI_2 of 1600 ms exceeds the longest gray-matter transit delay (cortical and subcortical) expected in healthy adults (Qiu et al., 2010), accommodating the slower flow which may be expected in certain older adults. Furthermore, the cortical and subcortical CBF reduction patterns in aging observed in this study differ spatially from the patterns of transit delay heterogeneity. Thus, it is not likely that the observed effects are driven primarily by acknowledged PASL-related artifacts and biases, although it is possible that arterial transit times may contribute in some way to the reported effects. Additionally, PASL measures of CBF are dependent on tissue and blood T_1 and T_2^*. In particular, T_2 reductions have been observed in HD (Chen et al., 1993; Vymazal et al., 2007). These changes have been attributed to iron accumulation. Notwithstanding, these changes were largely confined to the striatum, and with few existing studies in existence, it is unlikely that relaxation changes should decisively bias our perfusion findings. Finally, CBF and cortical thickness measurements inherently differ in their contrast-to-noise characteristics. This leads to spatially specific differences in sensitivity in CBF and atrophy measures, and should also be noted when interpreting the spatial distributions of the observed effects in a study such as this. In particular, it is well known that pulsed ASL data are SNR-challenged in subcortical white-matter, and although we limited ourselves to subcortical gray-matter structures, some of these regions are relatively more myelinated. However, we showed high cross-sessional reliability and robust HD-effects in these regions, suggesting that limited SNR was not a substantial confound here. An additional technical caveat pertains to challenges in obtaining robust tissue segmentation in certain regions of the brain (Fischl et al., 2002), particularly given the significant iron deposition (Qian and Wang, 1998) and atrophy in HD patients, which may confound tissue classification and result in volume-estimation biases through image intensity modulations and partial-volume effects. Such inaccuracies are expected to be more significant in structures with more non-uniform intensities. However, while such effects warrant careful interpretation of the data, they should be negligible in the majority of structures examined.

Summary

In summary, the current study provides a direct measure of HD-associated alterations in cerebral perfusion at an unprecedented level of spatial detail. This work highlights that reductions in cerebral

perfusion appear to be "uncoupled" from HD-related brain atrophy, and provides support for a role of regional hypoperfusion in neuronal dysfunction and early clinical symptoms. A great deal more work is necessary in order to fully elucidate the role of regionally selective alterations in CBF and HD pathology. The work described here may have broad reaching implications for our understanding of HD pathogenesis, progression and emerging therapies.

Supplementary materials related to this article can be found online at doi:10.1016/j.neuroimage.2011.08.112.

Acknowledgments

This research was supported by NIH grants R01NR010827, NS042861, NS058793, and P41RR14075, as well as by fellowship funding from the Canadian Institutes of Health Research (J. J. C.). We also thank Mr. Robert McInnis for aiding the neuropsychological assessments.

References

Adleman, N.E., Menon, V., Blasey, C.M., White, C.D., Warsofsky, I.S., Glover, G.H., Reiss, A.L., 2002. A developmental fMRI study of the Stroop color-word task. Neuroimage 16, 61–75.

Allen, K.L., Waldvogel, H.J., Glass, M., Faull, R.L., 2009. Cannabinoid (CB_1), $GABA_A$ and $GABA_B$ receptor subunit changes in the globus pallidus in Huntington's disease. J. Chem. Neuroanat. 37, 266–281.

Antonini, A., Leenders, K.L., Spiegel, R., Meier, D., Vontobel, P., Weigell-Weber, M., Sanchez-Pernaute, R., de Yebenez, J.G., Boesiger, P., Weindel, A., Maguire, R.P., 1996. Striatal glucose metabolism and dopamine D2 receptor binding in asymptomatic gene carriers and patients with Huntington's disease. Brain 119, 2085–2095.

Arai, K., Lo, E.H., 2009. An oligovascular niche: cerebral endothelial cells promote the survival and proliferation of oligodendrocyte precursor cells. J. Neurosci. 29, 4351–4355.

Asllani, I., Borogovac, A., Brown, T.R., 2008. Regression algorithm correcting for partial volume effects in arterial spin labeling MRI. Magn. Reson. Med. 60, 1362–1371.

Aston, J.A., Cunningham, V.J., Asselin, M.C., Hammers, A., Evans, A.C., Gun, R.N., 2002. Positronemission tomography partial volume correction: estimation and algorithms. J. Cereb. Blood Flow Metab. 22, 1019–1034.

Aylward, E.H., Li, Q., Stine, O.C., Ranen, N., Sherr, M., Barta, P.E., Bylsma, F.W., Pearlson, G.D., Ross, C.A., 1997. Longitudinal change in basal ganglia volume in patients with Huntington's disease. Neurology 48, 394–399.

Borghammer, P., Chakravarty, M., Jonsdottir, K.Y., Sato, N., Matsuda, H., Ito, K., Arahata, Y., Kato, T., Gjedde, A., 2010. Cortical hypometabolism and hypoperfusion in Parkinson's disease is extensive: probably even at early disease stages. Brain Struct. Funct. 214, 303–317.

Browne, S.E., Beal, M.F., 2006. Oxidative damange in Huntington's disease pathogenesis. Antioxid. Redox Signal. 8, 2061–2073.

Browne, S.E., Ferrante, R.J., Beal, M.F., 1999. Oxidative stress in Huntington's disease. Brain Pathol. 9, 147–163.

Buckner, R.L., Head, D., Parker, J., Fotenos, A.F., Marcus, D., Morris, J.C., Snyder, A.Z., 2004. A unified approach for morphometric and functional data analysis in young, old and demented adults using automated atlas-based head size normalization: reliability and validation against manual measurement of total intracranial volume. Neuroimage 23, 724–738.

Buckner, R.L., Snyder, A., Shannon, B.J., LaRossa, G., Sachs, R., Fotenos, A.F., Sheline, Y.I., Klunk, W.E., Mathis, C.A., Morris, J.C., Mintun, M.A., 2005. Molecular, structural, and functional characterizatioin of Alzheimer's disease: evidence for a relationship between default activity, amyloid, and memory. Neurobiol. Aging 25, 7709–7717.

Buxton, R.B., Frank, L.R., Wong, E.C., Siewert, B., Warach, S., Edelman, R.R., 1998. A general kinetic model for quantitative perfusion imaging with arterial spin labeling. Magn. Reson. Med. 40, 383–396.

Calamante, F., Thomas, D.L., Pell, G.S., Wiersma, J., Turner, R., 1999. Measuring cerebral blood flow using magnetic resonance imaging techniques. J. Cereb. Blood Flow Metab. 19, 701–735.

Cavuşoğlu, M., Pfeuffer, J., Uğurbil, K., Uludağ, K., 2009. Comparison of pulsed arterial spin labeling encoding schemes and absolute perfusion quantification. Magn. Reson. Imaging 27, 1039–1045.

Çavuşoğlu, M., Pfeuffer, J., Uğurbil, K., Uludağ, K., 2009. Comparison of pulsed arterial spin labeling encoding schemes and absolute perfusion quantification. Magn. Reson. Imaging. doi:10.1016/j.mri.2009.04.002.

Chen, J.C., Hardy, P.A., Kucharczyk, W., Clauberg, M., Joshi, J.G., Vourlas, A., Dhar, M., Henkelman, R.M., 1993. MR of human postmortem brain tissue: correlative study between T2 and assays of iron and ferritin in Parkinson and Huntington disease. AJNR Am. J. Neuroradiol. 14, 275–281.

Chen, J.J., Rosas, H.D., Salat, D.H., 2011. Reductions in cerebral blood flow in normal aging independent from brain atrophy. Neuroimage 55, 468–478.

Ciarmiello, A., Cannella, M., Lastoria, S., Simonelli, M., Frati, L., Rubinsztein, D.C., Squitieri, F., 2006a. Brain white-matter volume loss and glucose hypometabolism precede the clinical symptoms of Huntington's disease. J. Nucl. Med. 47, 215–222.

Ciarmiello, A., Cannella, M., Lastoria, S., Simonelli, M., Frati, L., Rubinsztein, D.C., Squitieri, F., 2006b. Brain white-matter volume loss and glucose hypometabolism precede the clinical symptoms of Huntington's disease. J. Nucl. Med. 47, 215–222.

Deckel, A.W., Cohen, D., Duckrow, R., 1998. Cerebral blood flow velocity decreases during cognitive stimulation in Huntington's disease. Neurology 51, 1576–1583.

Deckel, A.W., Weiner, R., Szigeti, D., Clark, V., Vento, J., 2000. Altered patterns of regional cerebral blood flow in patients with Huntington's disease:A SPECT study during rest and cognitive or motor activation. J. Nucl. Med. 41, 773–780.

Detre, J.A., Wang, J., Wang, Z., Rao, H., 2009. Arterial spin-labeled perfusion MRI in basic and clinical neuroscience. Curr. Opin. Neurol. 22, 348–355.

Donahue, M.J., Near, J., Blicher, J.U., Jezzard, P., 2010. Baseline GABA concentration and fMRI response. Neuroimage 53, 392–398.

Dugas, J.C., Mandemakers, W., Rogers, M., Ibrahim, A., Daneman, R., Barres, B.A., 2008. A novel purification method for CNS projection neurons leads to the identification of brain vascular cells as a source of trophic support for corticospinal motor neurons. J. Neurosci. 28, 8294–8305.

Feany, M.B., La Spada, A.R., 2003. Polyglutamines stop traffic: axonal transport as a common target in neurodegenerative diseases. Neuron 40, 1–2.

Feigin, A., Leenders, K.L., Moeller, J.R., Missimer, J., Kuenig, G., Spetsieris, P., Antonini, G.A., Eidelberg, D., 2001. Metabolic network abnormalities in early Huntington's disease: an [18F]FDG PET study. J. Nucl. Med. 42, 1591–1595.

Fischl, B., Dale, A.M., 2000. Measuring the thickness of the human cerebral cortex from magnetic resonance images. Proc. Natl. Acad. Sci. U. S. A. 97, 11050–11055.

Fischl, B., Sereno, M.I., Dale, A.M., 1999. Cortical surface-based analysis. II: inflation, flattening, and a surface-based coordinate system. Neuroimage 9, 195–207.

Fischl, B., Salat, D.H., Busa, E., Albert, M., Dieterich, M., Haselgrove, C., Van der Kouwe, A., Killiany, R., Kennedy, D., Klaveness, S., Montillo, A., Makris, N., Rosen, B., Dale, A.M., 2002. Whole brain segmentation: automated labeling of neuroanatomical structures in the human brain. Neuron 31, 341–355.

Fischl, B., Salat, D.H., van der Kouwe, A.J.W., Makris, N., Segonne, F., Quinn, B.T., Dale, A.M., 2004a. Sequence-independent segmentation of magnetic resonance images. Neuroimage 23, S69–S84.

Fischl, B., van der Kouwe, A., Destrieux, C., Halgren, E., Segonne, F., Salat, D.H., Busa, E., Seidman, L.J., Goldstein, J., Kennedy, D., Carviness, V., Makris, N., Rosen, B., Dale, A.M., 2004b. Automatically parcellating the human cerebral cortex. Cereb. Cortex 14, 11–22.

Ginovart, N., Lundin, A., Farde, L., Halldin, C., Backman, L., Swahn, C.-G., Pauli, S., Sedvall, G., 1997. PET study of the pre- and post-synaptic dopaminergic markers for the neurodegenerative process in Huntington's disease. Brain 120, 503–514.

Gonzalez-Zulueta, M., Ensz, L.M., Mukhina, G., Lebovitz, R.M., Zwacka, R.M., Engelhardt, J.F., Oberley, L.W., Dawson, V.L., Dawson, T.M., 1998. Manganese superaoxide dismutase protects nNOS neurons from NMDA and nitric oxide-mediated neurotoxicity. J. Neurosci. 18, 2040–2055.

Greve, D.N., Fischl, B., 2009. Accurate and robust brain image alignment using boundary-based registration. Neuroimage 48, 68–72.

Guo, S., Kim, W.J., Lok, J., Lee, S.R., Besancon, E., Luo, B.H., Stins, M.F., Wang, X., Dedhar, S., Lo, E.H., 2008. Neuroprotection via matrix-trophic coupling between cerebral endothelial cells and neurons. Proc. Natl. Acad. Sci. U. S. A. 105, 7582–7587.

Hagler, D.J., Saygin, A.P., Sereno, M.I., 2006. Smoothing and cluster thresholding for cortical surface-based group analysis of fMRI data. Neuroimage 33, 1093–1103.

Harris, G.J., Codori, A.M., Lewis, R.F., Schmidt, E., Bedi, A., Brandt, J., 1999. Reduced basal ganglia blood flow and volume in pre-symptomatic, gene-tested persons at-risk for Huntington's disease. Brain 122, 1667–1678.

Hasselbalch, S.G., Øberg, G., Sorensen, S.A., Andersen, A.R., Waldemar, G., Schmidt, J.F., Fenger, K., Paulson, O.B., 1992. Reduced regional cerebral blood flow in Huntington's disease studied by SPECT. J. Neurol. Neurosurg. Psychiatry 55, 1018–1023.

Hobbs, N.Z., Henley, S.M.D., Ridgway, G.R., Wild, E.J., Barker, R.A., Scahill, R.I., Barnes, J., Fox, N.C., Tabrizi, S.J., 2009. The progression of regional atrophy in premanifest and early Huntington's disease: a longitudinal voxel-based morphometry study. J. Neurol. Neurosurg. Psychiatry. doi:10.1136/jnnp. 2009.190702.

Huntington Study Group, 1996. Unified Huntington's Disease Rating Scale: reliability and consistency. Mov. Disord. 11, 136–142.

Iadecola, C., 2003. Cerebrovascular effects of amyloid-beta peptides: mechanisms and implications for Alzheimer's dementia. Cell. Mol. Neurobiol. 23, 681–689.

Jech, R., Klempır, J., Vymazal, J., Zidovska, J., Klempırova, O., Ruzicka, E., Roth, J., 2007. Variation of selective gray and white matter atrophy Huntington's disease. Mov. Disord. 22, 1783–1789.

Jernigan, T.L., Salmon, D.P., Butters, N., Hesselink, J.R., 1991. Cerebral structure on MRI, part II: specific changes in Alzheimer's and Huntington's diseases. Biol. Psychiatry 29, 68–81.

Jurgens, C.K., van de Wiel, L., van Es, A.C., Grimbergen, Y.M., Witjes-Ané, M.N., van der Grond, J., Middelkoop, H.A., Roos, R.A., 2008. Basal ganglia volume and clinical correlates in 'preclinical' Huntington's disease. J. Neurol. 255, 1785–1791.

Kassubek, J., Juengling, F.D., Ecker, D., Landwehrmeyer, G.B., 2005. Thalamic atrophy in Huntington's disease co-varies with cognitive performance: a morphometric MRI analysis. Cereb. Cortex 15, 846–853.

Kim, J., Amante, D.J., Moody, J.P., Edgerly, C.K., Bordiuk, O.L., Smith, K., Matson, S.A., Matson, W.R., Scherzer, C.R., Rosas, H.D., Hersch, S.M., Ferrante, R.J., 2010a. Reduced creatine kinase as a central and peripheral biomarker in Huntington's disease. 40th Meeting of the Foundation of Hereditary Diseases, Boston, p. 9.

Kim, J., Moody, J.P., Edgerly, C.K., Bordiuk, O.L., Cormier, K., Smith, K., Beal, M.F., Ferrante, R.J., 2010b. Mitochondrial loss, dysfunction and altered dynamics in Huntington's disease. Hum. Mol. Genet. 19, 3919–3935.

Kuwert, T., Noth, J., Scholz, D., Schwarz, M., Lange, H.W., Topper, R., Herzog, H., Aulich, A., Feinendegen, L.E., 1993. Comparison of somatosensory evoked potentials with striatal glucose consumption measured by positron emission tomography in the early diagnosis of Huntington's disease. Mov. Disord. 8, 98–106.

Lee, C., Lopez, O.L., Becker, J.T., Raji, C., Dai, W., Kuller, L.H., Gach, H.M., 2009. Imaging cerebral blood flow in the cognitively normal aging brain with arterial spin labeling: implications for imaging of neurodegenerative disease. J. Neuroimaging 19, 344–352.
Leenders, K.L., Perani, D., Lammertsma, A.A., Heather, J.D., Buckingham, P., Healy, M.J.R., Gibbs, J.M., Wise, R.J.S., Hatazawa, J., Herold, S., Beaney, R.P., Brooks, D.J., Spinks, T., Rhodes, C., Frackowiak, R.S., Jones, T., 1990. Cerebral blood flow, blood volume and oxygen utilization. Brain 113, 24–47.
Lemiere, J., Decruyenaere, M., Evers-Kiebooms, G., Vandenbussche, E., Dom, R., 2004. Cognitive changes in patients with Huntington's disease (HD) and asymptomatic carriers of the HD mutation — a longitudinal follow-up study. J. Neurol. 251, 935–942.
Lu, H., Donahue, M.J., van Zijl, P.C.M., 2006. Detrimental effects of BOLD signal in arterial spin labeling fMRI at high field strength. Magn. Reson. Med. 56, 546–552.
Ma, Y., Eidelberg, D., 2007. Functional imaging of cerebral blood flow and glucose metabolism in Parkinson's disease and Huntington's disease. Mol. Imaging Biol. 9, 223–233.
MacIntosh, B.J., Filippini, N., Chappell, M.A., Woolrich, M.W., Mackay, C.E., Jezzard, P., 2010. Assessment of arterial arrival times derived from multiple inversion time pulsed arterial spin labeling MRI. Magn. Reson. Med. 63, 641–647.
Nopoulos, P.C., Aylward, E.H., Ross, C.A., Johnson, H.J., Magnotta, V.A., Juhl, A.R., Pierson, R.K., Mills, J., Langbehn, D.R., Paulsen, J.S., PREDICT-HD-Investigators-Coordinators-of-Huntington-Study-Group, 2010. Cerebral cortex structure in prodromal Huntington disease. Neurobiol. Dis. 40, 544–554.
Politis, M., Pavese, N., Tai, Y.F., Kiferle, L., Mason, S.L., Brooks, D.J., Tabrizi, S.J., Barker, R.A., Piccini, P., 2011. Microglial activation in regions related to cognitive function predicts disease onset in Huntington's disease: a multimodal imaging study. Hum. Brain Mapp. 32, 258–270.
Powers, W.J., Videen, T.O., Markham, J., McGee-Minnich, L., Antenor-Dorsey, J.V., Hershey, T., Perlmutter, J.S., 2007. Selective defect of in vivo glycolysis in early Huntington's disease striatum. Proc. Natl. Acad. Sci. U. S. A. 104, 2945–2949.
Qian, Z.M., Wang, Q., 1998. Expression of iron transport proteins and excessive iron accumulation in the brain in neurodegenerative disorders. Brain Res. Brain Res. Rev. 27, 257–267.
Qiu, M., Maguire, R.P., Arora, J., Planeta-Wilson, B., Weinsimmer, D., Wang, J., Wang, Y., Kim, H., Rajeevan, N., Huang, Y., Carson, R.E., Constable, R.T., 2010. Arterial transit time effects in pulsed arterial spin labeling CBF mapping: insight from a PET and MR study in normal human subjects. Magn. Reson. Med. 63, 374–384.
Ravina, B., Romer, M., Constantinescu, R., Biglan, K., Brocht, A., Kieburtz, K., Shoulson, I., McDermott, M.P., 2008. The relationship between CAG repeat length and clinical progression in Huntington's disease. Mov. Disord. 23, 1223–1227.
Reijonen, S., Kukkonen, J.P., Hyrskyluoto, A., Kivinen, J., Kairisalo, M., Takei, N., Lindholm, D., Korhonen, L., 2010. Downregulation of NF-kappaB signaling by mutant huntingtin proteins induces oxidative stress and cell death. Cell. Mol. Life Sci. 67, 1929–1941.
Rosas, H.D., Koroshetz, W.J., Chen, Y.I., Skeuse, C., Vangel, M., Cudkowicz, M.E., Caplan, K., Marek, K., Seidman, L.J., Makris, N., Jenkins, B.G., Goldstein, J.M., 2003. Evidence for more widespread cerebral pathology in early HD: an MRI-based morphometric analysis. Neurology 60, 1615–1620.
Rosas, H.D., Hevelone, N.D., Zaleta, A.K., Greve, D.N., Salat, D.H., Fischl, B., 2005. Regional cortical thinning in preclinical Huntington disease and its relationship to cognition. Neurology 65, 745.
Rosas, H.D., Salat, D.H., Lee, S., Zaleta, A.K., Pappu, V., Fischl, B., Greve, D.N., Hevelone, N., Hersch, S.M., 2008. Cerebral cortex and the clinical expression of Huntington's disease: complexity and heterogeneity. Brain 131, 1057–1068.
Ruocco, H.H., Bonilha, L., Li, L.M., Lopes-Cendes, I., Cendes, F., 2010. Huntington disease: effects of the length of the expanded CAG repeat. J. Neurol. Neurosurg. Psychiatry 79, 130–135.
Salat, D.H., Chen, J.J., van der Kouwe, A.J., Greve, D.N., Fischl, B., Rosas, H.D., 2011. Hippocampal degeneration is associated with temporal and limbic gray matter/white matter tissue contrast in Alzheimer's disease. Neuroimage 54, 1795–1802.
Sax, D.S., Powsner, R., Kim, A., Tilak, S., Bhatia, R., Cupples, L.A., Myers, R.H., 1996. Evidence of cortical metabolic dysfunction in early Huntington's disease by single-photon-emission computed tomography. Mov. Disord. 11, 671–677.
Segonne, F., Dale, A.M., Busa, E., Glessner, M., Salat, D., Hahn, H.K., Fischl, B., 2004. A hybrid approach to the skull stripping problem in MRI. Neuroimage 22, 1060–1075.
Segonne, F., Pacheco, J., Fischl, B., 2007. Geometrically accurate topology-correction of cortical surfaces using nonseparating loops. IEEE Trans. Med. Imaging 26, 518–529.
Selemon, L.D., Rajkowska, G., Goldman-Rakic, P.S., 2004. Evidence for progression in frontal cortical pathology in late-stage Huntington's disease. J. Comp. Neurol. 468, 190–204.
Shin, W., Horowitz, S., Ragin, A., Chen, Y., Walker, M., Caroll, T.J., 2007. Quantitative cerebral perfusion using dynamic susceptibility contrast MRI: evaluation of reproducibility and age- and gender-dependence with fully automated image postprocessing algorithm. Magn. Reson. Med. 58, 1232–1241.
Sled, J.G., Zijdenbos, A.P., Evans, A.C., 1998. A nonparametric method for automatic correction of intensity nonuniformity in MRI data, 17, pp. 87–97.
Sotrel, A., Paskevich, P.A., Kiely, D.K., Bird, E.D., Williams, R.S., Myers, R.H., 1991. Morphometric analysis of the prefrontal cortex in Huntington's disease. Neurology 41, 1117–1123.
Squitieri, F., Gellera, C., Cannella, M., Mariotti, C., Cislaghi, G., Rubinsztein, D.C., Almqvist, E.W., Turner, D.A., Bachoud-Levi, A.C., Simpson, S.A., Delatycki, M., Maglione, V., Hayden, M.R., Donato, S.D., 2003. Homozygosity for CAG mutation in Huntington disease is associated with a more severe clinical course. Brain 126, 946–955.
Stoffers, D., Sheldon, S., Kuperman, J.M., Goldstein, J., Corey-Bloom, J., Aron, A.R., 2010. Contrasting gray and white matter changes in preclinical Huntington disease: an MRI study. Neurology 74, 1208–1216.
Tanahashi, N., Meyer, J.S., Ishikawa, Y., Kandula, P., Mortel, K.F., Rogers, R.L., 1985. Cerebral blood flow and cognitive testing correlates in Huntington's disease. Acta Neurol. 42, 1169–1175.
Théberge, J., 2008. Perfusion magnetic resonance imaging in psychiatry. Top. Magn. Reson. Imaging 19, 111–130.
Tosun, D., Mojabi, P., Weiner, M.W., Schuff, N., 2010. Joint analysis of structural and perfusion MRI for cognitive assessment and classification of Alzheimer's disease and normal aging. Neuroimage. doi:10.1016/j.neuroimage.2010.04.033.
Underwood, B.R., Imarisio, S., Fleming, A., Rose, C., Krishna, G., Heard, P., Quick, M., Korolchuk, V.I., Renna, M., Sarkar, S., García-Arencibia, M., O'Kane, C.J., Murphy, M.P., Rubinsztein, D.C., 2010. Antioxidants can inhibit basal autophagy and enhance neurodegeneration in models of polyglutamine disease. Hum. Mol. Genet. 19, 3413–3429.
van den Bogaard, S.J., Dumas, E.M., Acharya, T.P., Johnson, H., Langbehn, D.R., Scahill, R.I., Tabrizi, S.J., van Buchem, M.A., van der Grond, J., Roos, R.A., TRACK-HD-Investigator-Group, 2011. Early atrophy of pallidum and accumbens nucleus in Huntington's disease. J. Neurol. 258, 412–420.
van der Kouwe, A.J.W., Benner, T., Salat, D.H., Fischla, B., 2008. Brain morphometry with multiecho MPRAGE. Neuroimage 40, 559–569.
Varga, A.W., Johnson, G., Babb, J.S., Herbert, J., Grossman, R.I., Inglese, M., 2009. White matter hemodynamic abnormalities precede sub-cortical gray matter changes in multiple sclerosis. J. Neurol. Sci. 282, 28–33.
Vymazal, J., Klempír, J., Jech, R., Zidovská, J., Syka, M., Růzicka, E., Roth, J., 2007. MR relaxometry in Huntington's disease: correlation between imaging, genetic and clinical parameters. J. Neurol. Sci. 263, 20–25.
Walker, F.O., 2007. Huntington's disease. Lancet 369, 218–228.
Wang, J., Alsop, D.C., Li, L., Listerud, J., Gonzalez-At, J.B., Schnall, M.D., Detre, J.A., 2002. Comparison of quantitative perfusion imaging using arterial spin labeling at 1.5 and 4.0 Tesla. Magn. Reson. Med. 48, 242–254.
Weinberger, D.R., Berman, K.F., Iadarola, M., Driesen, N., Zec, R.F., 1988. Prefrontal cortical blood flow and cognitive function in Huntington's disease. J. Neurol. Neurosurg. Psychiatry 51, 94–104.
Wild, E.J., Henley, S.M.D., Hobbs, N.Z., Frost, C., MacManus, D.G., Barker, R.A., Fox, N.C., Tabrizi, S.J., 2009. Rate and acceleration of whole-brain atrophy in premanifest and early Huntington's disease. Mov. Disord. 25, 888–895.
Wong, E.C., Buxton, R.B., Frank, L.R., 1998a. Quantitative imaging of perfusion using a single subtraction (QUIPSS and QUIPSS II). Magn. Reson. Med. 39, 702–708.
Wong, E.C., Buxton, R.B., Frank, L.R., 1998b. A theoretical and experimental comparison of continuous and pulsed arterial spin labeling techniques for quantitative perfusion imaging. Magn. Reson. Med. 40, 348–355.
Worsley, K.J., Taylor, J.E., Tomaiuolo, F., Lerch, J., 2004. Unified univariate and multivariate random field theory. Neuroimage 23 (Suppl 1), S189–S195.
Ye, F.Q., Mattay, V.S., Jezzard, P., Frank, J.A., Weinberger, D.R., McLaughlin, A.C., 1997. Correction for vascular artifacts in cerebral blood flow values measured by using arterial spin tagging techniques. Magn. Reson. Med. 37, 226–235.
Zou, Q., Wu, C.W., Stein, E.A., Zang, Y., Yang, Y., 2009. Static and dynamic characteristics of cerebral blood flow during the resting state. Neuroimage 48, 515–524.